On the computation of ground state and dynamics of Schrödinger-Poisson-Slater system

Yong Zhang[a], Xuanchun Dong[b,*]

[a] *Department of Mathematical Sciences, Tsinghua University, Beijing, 100084, P.R. China.*
[b] *Department of Mathematics and Center for Computational Science and Engineering, National University of Singapore, 119076, Singapore.*

Abstract

In this paper, we deal with the computation of ground state and dynamics of the Schrödinger-Poisson-Slater (SPS) system. To this end, backward Euler and time-splitting pseudospectral methods are proposed for the nonlinear Schrödinger equation with the nonlocal Hartree potential approximated by solving a Poisson equation. The approximation approaches for the Hartree potential include fast convolution algorithms, which are accelerated by using FFT in 1D and fast multipole method (FMM) in 2D and 3D, and sine/Fourier pseudospectral methods. The inconsistency in 0-mode in Fourier pseudospectral approach is pointed out, which results in a significant loss of high-order of accuracy as expected for spectral methods. Numerical comparisons show that in 1D the fast convolution and sine pseudospectral approaches are compatible. While, in 3D the fast convolution approach based on FMM is second-order accurate and the Fourier pseudospectral approach is better than it from both efficiency and accuracy point of view. Among all these approaches, the sine pseudospectral one is the best candidate in the numerics of the SPS system. Finally, we apply the backward Euler and time-splitting sine pseudospectral methods to study the ground state and dynamics of 3D SPS system in different setups.

Keywords:
Schrödinger-Poisson-Slater system, Schrödinger-Poisson type system, ground state, backward Euler pseudospectral method, time-splitting pseudospectral method, fast convolution

1. Introduction

The Schrödinger-Poisson-Slater (SPS) system, also named as the Schrödinger-Poisson-Xα system, is a local single particle approximation of the time-dependent Hartree-Fock equations. It reads, in scaled form,

$$i\,\partial_t\psi(\mathbf{x},t) = \left[-\frac{1}{2}\nabla^2 + V_{\rm ext}(\mathbf{x}) + C_P\,V_P(\mathbf{x},t)\; - \alpha\;|\psi|^{\frac{2}{d}}\right]\psi, \quad \mathbf{x}\in\mathbb{R}^d, \quad t>0, \tag{1.1}$$

$$\nabla^2 V_P(\mathbf{x},t) = -|\psi|^2, \qquad \mathbf{x}\in\mathbb{R}^d, \quad t>0, \tag{1.2}$$

$$\psi(\mathbf{x},t=0) = \psi_0(\mathbf{x}), \qquad \mathbf{x}\in\mathbb{R}^d. \tag{1.3}$$

*Corresponding author.
Email addresses: zhangyong07@mails.tsinghua.edu.cn (Yong Zhang), dong.xuanchun@nus.edu.sg (Xuanchun Dong)

Here, the complex-valued function $\psi(\mathbf{x},t)$ with $\lim_{|\mathbf{x}|\to\infty}|\psi(\mathbf{x},t)|=0$ stands for the single particle wave function, $V_{\rm ext}(\mathbf{x})$ is a given external potential, for example a confining potential, $V_P(\mathbf{x},t)$ denotes the Hartree potential with free-space condition, and C_P and α are interaction constants. The sign of Poisson constant C_P depends on the type of interaction considered: $C_P>0$ in the repulsive case and $C_P<0$ in the attractive case. Physically, the Slater constant $\alpha>0$ for electrons. Note that if the Slater term is not considered, i.e. $\alpha=0$, then the SPS system (1.1)-(1.3) coincides with the Schrödinger-Poisson (SP) system. Also, the attractive SP system, i.e. (1.1)-(1.3) with $C_P<0$ and $\alpha=0$, is usually called the Schrödinger-Newton (SN) system which describes the particle moving in its own gravitational potential. Hence, throughout this paper we assume $\alpha\geq 0$ and so the arguments and results in this work are applicable to the SP and SN systems as well.

First we sketch the formal derivation of the SPS system as an effective approximation of a quantum system of N electrons interacting via Coulomb potential, with a local exchange correction term to the so-called mean-field approximation. To obtain the mean-field approximation, the Hartree ansatz for the N-particle wave function yields the SP system ($\alpha=0$ in (1.1)), for which rigorous derivations were given recently in [1] for the stationary case, and respectively, in [2] for the time-dependent case. However, the Hartree ansatz writes the N-particle wave function as a simple product of one-particle wave functions; hence, in the SP model the "Pauli exclusion principle" is disregarded and the exchange effects of electrons are missing. In contrast, the Hartree-Fock (HF) ansatz takes the N-particle wave function as a Slater determinant, which vanishes for two particles occupying the same position, and thus realizes the antisymmetrization of the N-particle wave function so that the Pauli principle is respected. In the context of minimizing the total energy of a N-body system, with the HF ansatz the original N-body problem reduces to a system of N coupled stationary one-electron Schrödinger equations. This HF model has been used to analyze vast phenomena in quantum chemistry and solid state physics. For the rigorous analysis of the stationary HF system we refer to [32] and references therein. For the time-dependent case, the HF equations formulated for the density matrix were rigorously derived by means of "mean field limits" in [3] for the bounded interactions and, respectively, in [4] for the Coulomb case.

The HF equations are too complex for numerical simulations since the nonlocal exchange term is quite costly to calculate. Slater in [37] gave one simple approximation to the exchange term, which is proportional to $\rho^\alpha\psi_j$ with $\alpha=1/3$. Here, $\rho(\mathbf{x}):=\sum_{j=1}^N|\psi_j(\mathbf{x})|^2$ is the local density and ψ_j is one-particle wave function. This local expression was actually first introduced implicitly by Dirac while considering the exchange energy as a correction in the Thomas-Fermi model [21]. Such kind of ρ^α approximation is usually named as Xα-approach, in which α is taken as a parameter and differs as various limits. Such local approximation to the nonlocal HF exchange potential provides excellent results in the study of stationary states [22, 29, 31]. The rigorous derivations of this Xα approximation in the stationary case were given in [13, 14] and the argument in time-dependent case is still an active topic. Therefore, so far only the SP system has been rigorously derived as the time-dependent one particle approximation. Hence, it is imperative to find appropriate corrections to the mean-field potential in the SP model so as to take into account the exchange effects. To this end, adding the local Xα-approximated exchange term (with $\alpha=1/d$ for the problem in $d=1,2,3$ space dimensions according to the derivation in [3]) to the effective potential in the SP model, the SPS system was proposed in [34].

The SPS system (1.1)-(1.3) is equivalent to a nonlinear Schrödinger (NLS) equation,

$$i\,\partial_t\psi(\mathbf{x},t) = \left[-\frac{1}{2}\nabla^2 + V_{\rm ext}(\mathbf{x}) + C_P V_P\left(|\psi|^2\right) - \alpha\,|\psi|^{\frac{2}{d}}\right]\psi, \quad \mathbf{x}\in\mathbb{R}^d, \quad t>0. \tag{1.4}$$

Here we rewrite the Hartree potential V_P as a function of $|\psi|^2$

$$V_P\left(|\psi|^2\right) = G_d(|\mathbf{x}|) * |\psi|^2, \tag{1.5}$$

where $G_d(|\mathbf{x}|)$ denotes the Green's function of the Laplacian on $\mathbb{R}^d$

$$G_d(|\mathbf{x}|) = \begin{cases} -\frac{1}{2}|\mathbf{x}|\,, & d=1,\\ -\frac{1}{2\pi}\ln(|\mathbf{x}|)\,, & d=2,\\ \frac{1}{4\pi}|\mathbf{x}|^{-1}\,, & d=3. \end{cases} \tag{1.6}$$

There are at least two important invariants of (1.4): the *mass of particles*

$$N(\psi) := \|\psi(\mathbf{x},t)\|^2 = \int_{\mathbb{R}^d} |\psi(\mathbf{x},t)|^2\,d\mathbf{x}, \tag{1.7}$$

which is convenient to be normalized to unity, and the *total energy*

$$E(\psi) := \int_{\mathbb{R}^d}\left[\frac{1}{2}|\nabla\psi|^2 + \left(V_{\rm ext}(\mathbf{x}) + \frac{C_P}{2}V_P(|\psi|^2)\right)|\psi|^2 - \alpha\frac{d}{d+1}|\psi|^{\frac{2}{d}+2}\right]d\mathbf{x}. \tag{1.8}$$

The NLS equations have drawn lots of attention to mathematicians, and for an overview of this subject we refer to [16, 17, 40]. Also, there is a series of analytical results on the SPS system in literatures. For (1.4), by the standard results in [17] the global existence of a unique solution in its energy space H^1 can be established for 3D [13]. The existence theory in 1D was given in [38] and the analysis in 2D was recently announced in [33]. Another interesting problem is the existence and uniqueness of ground states, i.e. the solutions which minimize the total energy under the normalization constraint. For the most simple-looking system in form of (1.1)-(1.3), i.e. the SN system without external potential, the existence of a unique spherically symmetric ground state in 3D was proven by Lieb in [30], and in any dimension $d \le 6$ was given in [20]. There is no global minimum of the energy functional for the repulsive SP system without potential since the infimum of its energy is always zero. When the Slater term in (1.4) is considered but in the absence of any external potential, the existence analysis of ground state in 3D was given in [35], and in particular the existence of a unique spherically symmetric ground state is proven in [15] for the attractive case. To our knowledge, so far the existence analysis of higher bound states remains open.

Along the numerical aspect, self-consistent solutions of the SPS system are important in the simulations of a quantum system. For example, time-independent SP system was solved in [12, 18] for the eigenstates of the quantum system, and time-dependent spherically symmetric SP system was considered in [23] and time-dependent SN system was treated in [27] with three kinds of symmetry: spherical, axial and translational symmetry. Most of the pervious work apply Crank-Nicholson time integration and finite difference for space discretization. Note that in general the ground state of the SPS system will lose the symmetric profile due to the external potential and therefore we cannot obtain a reduced quasi-1D model from (1.1)-(1.3) as for the SN system [27]. On the other hand, the computation of stationary states and dynamics of the NLS equation (1.4) without Hartree potential

(also named as Gross-Pitaevskii equation (GPE)), has been intensively studied. Among the numerical methods proposed in literatures, discretizations based on a gradient flow with discrete normalization (GFDN) [6, 7] prove more efficient in finding the ground and excited states of GPE modeling the Bose-Einstein condensates. For dynamics, a time-splitting pseudospectral discretization [9, 10, 11] shows its accuracy and efficiency in practice. Such results suggest that we can extend these successful ideas to the computation of ground state and dynamics of the SPS system. For example, similar methods were extended in [5] to treat a Gross-Pitaevskii-Poisson type system, and a time-splitting approach was used in [8] for computing the dynamics of the SPS system with periodic boundary conditions in all space dimensions. However, there still remains an issue that how to approximate the Hartree potential (1.5) properly, which definitely affects the overall accuracy and efficiency.

The aim of this paper is to design and compare different numerical methods for computing the ground state and dynamics of the SPS system. The methods proposed combine various numerical approximations of (1.5) with a backward Euler pseudospectral scheme to discretize the GFDN of the SPS system to compute its ground state, and with a time-splitting pseudospectral method to simulate its dynamics. The methods for computing the Hartree potential (1.5) considered in this paper include the convolution methods which approximate the convolution in (1.5) directly, and pseudospectral methods based on sine and Fourier base functions. The convolution methods are implemented by fast algorithms with the help of FFT in 1D and, respectively, fast multipole method (FMM) in 2D and 3D. The pseudospectral methods for solving (1.2) are formulated in standard way and the inconsistency in 0-mode of Fourier approach is pointed out, which results in a significant loss of expected spectral accuracy for spectral-type methods.

The paper is organized as follows. In Section 2 we give the GFDN of the SPS system and in Section 3 we present different numerical methods for computing the ground state. In Section 4, methods based on time-splitting time integration are proposed for computing the dynamics. In section 5, numerical comparison results on the ground state and dynamics are reported and the application results are also shown. Finally, some closing remarks are drawn in the last section. Throughout this paper, we adopt the standard Sobolev spaces and their corresponding norms.

2. Ground state and normalized gradient flow

To find the stationary states of (1.1)-(1.3), we take the ansatz

$$\psi(\mathbf{x},t) = e^{-i\mu t}\phi(\mathbf{x}), \qquad \mathbf{x}\in\mathbb{R}^d, \quad t\geq 0, \tag{2.1}$$

where $\mu\in\mathbb{R}$ is the chemical potential and $\phi := \phi(\mathbf{x})$ is a time-independent function with $\lim_{|\mathbf{x}|\to\infty}|\phi(\mathbf{x})| = 0$. Inserting (2.1) into (1.1)-(1.3), we get the time-independent Schrödinger equation (or a nonlinear eigenvalue problem)

$$\mu\,\phi(\mathbf{x}) = \left[-\frac{1}{2}\nabla^2 + V_{\rm ext}(\mathbf{x}) + C_P V_P(|\phi|^2) - \alpha|\phi|^{\frac{2}{d}}\phi\right]\phi, \qquad \mathbf{x}\in\mathbb{R}^d, \tag{2.2}$$

under the constraint

$$\|\phi\|^2 := \int_{\mathbb{R}^d}|\phi(\mathbf{x})|^2\,d\mathbf{x} = 1. \tag{2.3}$$

Here $V_P\left(|\phi|^2\right)$ satisfies (1.5). Mathematically the ground state is defined as the minimizer of the following nonconvex minimization problem:

Find $\phi_g \in S$ and $\mu_g \in \mathbb{R}$ such that

$$E^g := E(\phi_g) = \min_{\phi \in S} E(\phi), \qquad \mu^g := \mu(\phi_g), \tag{2.4}$$

where the constraint set S is defined as $S := \left\{\phi \mid \|\phi\|^2 = 1,\ E(\phi) < \infty\right\}$ and the chemical potential (or eigenvalue of (2.2)) is defined as

$$\begin{aligned}\mu(\phi) &:= \int_{\mathbb{R}^d} \left[\frac{1}{2}|\nabla\phi|^2 + V_{\rm ext}(\mathbf{x})|\phi|^2 + C_P V_P(|\phi|^2)|\phi|^2 - \alpha|\phi|^{\frac{2}{d}}|\phi|^2\right] d\mathbf{x} \\ &\equiv E(\phi) + \int_{\mathbb{R}^d} \left[\frac{C_P}{2} V_P(|\phi|^2)|\phi|^2 - \alpha\frac{1}{d+1}|\phi|^{\frac{2}{d}+2}\right] d\mathbf{x}. \end{aligned} \tag{2.5}$$

In above the energy functional $E(\phi)$ is defined according to (1.8). In fact, only the positive solution of (2.4) is of interests since for any $\phi(\mathbf{x}) \in S$ we always have $E(\phi) \geq E(|\phi|)$. Also, the nonlinear eigenvalue problem (2.2) under the constraint (2.3) can be viewed as the Euler-Lagrangian equation of the nonconvex minimization problem (2.4). Any eigenfunction of (2.2) under the constraint (2.3) corresponds to the critical point of energy functional $E(\phi)$ over the unite sphere S, whose energy is larger than E^g is usually called as an excited state in physics literatures.

In order to solve the minimization problem (2.4) numerically, we construct the gradient flow with discrete normalization (GFDN) via the similar procedure as in [7] for computing the stationary states of a GPE. Choose a time step $\Delta t > 0$ and set $t_n = n\,\Delta t$ for $n = 0, 1, \ldots$. Applying the steepest decent method to the energy functional $E(\phi)$ in (1.8) without the constraint (2.3), and then projecting the solution back to the unit sphere S at the end of each time interval $[t_n, t_{n+1}]$ to enforce the constraint (2.3), we obtain the following gradient flow for $\phi(\mathbf{x}, t)$ with discrete normalization:

$$\partial_t \phi(\mathbf{x}, t) = -\frac{1}{2}\frac{\delta E(\phi)}{\delta \phi} = \left[\frac{1}{2}\nabla^2 - V_{\rm ext}(\mathbf{x}) - C_P V_P(|\phi|^2) + \alpha|\phi|^{\frac{2}{d}}\right]\phi, \tag{2.6}$$

$$\phi(\mathbf{x}, t_{n+1}) := \phi(\mathbf{x}, t_{n+1}^+) = \frac{\phi(\mathbf{x}, t_{n+1}^-)}{\|\phi(\mathbf{x}, t_{n+1}^-)\|}, \tag{2.7}$$

$$\lim_{|\mathbf{x}|\to\infty} |\phi(\mathbf{x}, t)| = 0, \quad \phi(\mathbf{x}, 0) = \phi_0(\mathbf{x}), \quad \text{with} \quad \|\phi_0\| = 1, \tag{2.8}$$

for $\mathbf{x} \in \mathbb{R}^d$, $t_n \leq t < t_{n+1}$ and $n \geq 0$, where $\phi(\mathbf{x}, t_n^\pm) := \lim_{t\to t_n^\pm} \phi(\mathbf{x}, t)$. In fact, the gradient flow (2.6) can also be obtained from the NLS equation (1.4) by setting time t to $\tau = i\,t$, which refers to the imaginary time method in physics literatures.

Letting $\Delta t \to 0$ in the GFDN (2.6)-(2.8), we obtain the following continuous normalized gradient flow (CNGF) [7]:

$$\partial_t \phi(\mathbf{x}, t) = \left[\frac{1}{2}\nabla^2 - V_{\rm ext}(\mathbf{x}) - C_P V_P(|\phi|^2) + \alpha|\phi|^{\frac{2}{d}} + \frac{\mu(\phi)}{\|\phi\|^2}\right]\phi, \tag{2.9}$$

$$\lim_{|\mathbf{x}|\to\infty} |\phi(\mathbf{x}, t)| = 0, \quad \phi(\mathbf{x}, 0) = \phi_0(\mathbf{x}), \quad \text{with} \quad \|\phi_0\| = 1, \tag{2.10}$$

for $\mathbf{x} \in \mathbb{R}^d$ and $t \geq 0$, where $\mu(\phi)$ is defined by (2.5). It can be justified by direct calculation that the CNGF (2.9)-(2.10) is normalization conserved and energy diminishing, i.e.,

$$\|\phi(\mathbf{x}, t)\|^2 \equiv \|\phi_0\|^2 = 1, \qquad \frac{d}{dt}E(\phi(\mathbf{x}, t)) = -2\|\phi_t(\mathbf{x}, t)\|^2 \leq 0, \qquad t \geq 0,$$

which also implies that $E(\phi(\mathbf{x},t_2)) \le E(\phi(\mathbf{x},t_1))$ for $0 \le t_1 \le t_2 < \infty$.

The positive ground state $\phi_g(\mathbf{x})$ and its corresponding chemical potential μ_g can be obtained from the stationary solution of GFDN (2.6)-(2.8) or CNGF (2.9)-(2.10) with a positive initial condition $\phi_0(\mathbf{x}) \ge 0$.

3. Numerical methods for computing ground state

In this section, we shall present numerical methods for computing the ground state. Our starting model is the GFDN (2.6)-(2.8) constructed in finding the ground state.

3.1. Backward Euler spectral/pseudospectral discretization

In practice, the whole space problem (2.6)-(2.8) is usually truncated into a bounded computation domain Ω with homogeneous Dirichlet or periodic boundary conditions. We choose Ω as an interval $[a,b]$ in 1D, a rectangle $[a,b]\times[c,d]$ in 2D, a box $[a,b]\times[c,d]\times[e,f]$ in 3D. For simplicity of notation we shall introduce the discretization in 1D. Generalization to higher dimensions is straightforward due to tensor product grids. When $d=1$, for $x \in [a,b]$, $t_n \le t < t_{n+1}$ and $n \ge 0$, we have

$$\partial_t \phi(x,t) = \frac{1}{2}\partial_{xx}\phi - V_{\rm ext}(x)\phi - C_P V_P(|\phi|^2)\phi + \alpha|\phi|^{\frac{2}{d}}\phi, \tag{3.1}$$

$$\phi(x,t_{n+1}) := \phi(x,t_{n+1}^+) = \frac{\phi(x,t_{n+1}^-)}{\|\phi(x,t_{n+1}^-)\|_{L^2(a,b)}}, \tag{3.2}$$

$$\phi(x,0) = \phi_0(x), \quad \text{with} \quad \|\phi_0\|^2_{L^2(a,b)} := \int_a^b |\phi_0(x)|^2 dx = 1, \tag{3.3}$$

with homogeneous Dirichlet boundary conditions:

$$\phi(a,t) = \phi(b,t) = 0, \qquad t > 0 \tag{3.4}$$

or periodic boundary conditions:

$$\phi(a,t) = \phi(b,t), \quad \phi_x(a,t) = \phi_x(b,t), \qquad t > 0. \tag{3.5}$$

We choose the spatial mesh size $h = \Delta x > 0$ with $h = \frac{(b-a)}{M}$ for M being an even positive integer, and let the grid points be $x_j = a + jh, j = 0,1,\ldots,M$. Define two function spaces

$$Y_M^{\mathcal{S}} = \text{span}\left\{\sin\left(\mu_l(x-a)\right),\ l = 1,\ldots,M-1,\ x \in [a,b]\right\},$$

$$Y_M^{\mathcal{F}} = \text{span}\left\{\exp\left(i\lambda_l\,(x-a)\right),\ l = -M/2,\ldots,M/2-1,\ x \in [a,b]\right\},$$

with

$$\mu_l = \frac{\pi l}{b-a} \quad (l = 1,\ldots,M-1), \qquad \lambda_l = \frac{2\pi l}{b-a} \quad (l = -M/2,\ldots,M/2-1).$$

Let $P_M^{\mathcal{S}} : Y_0 := \{U(x) \in C(a,b)\,|\,U(a) = U(b) = 0\} \to Y_M^{\mathcal{S}}$ and $P_M^{\mathcal{F}} : Y_{\rm p} := \{U(x) \in C(a,b)\,|\,U(a) = U(b), U'(a) = U'(b)\} \to Y_M^{\mathcal{F}}$ be the standard projection operators [36], i.e.,

$$\left(P_M^{\mathcal{S}}(U)\right)(x) = \sum_{l=1}^{M-1} \widehat{(U)}_l^{\mathcal{S}} \sin\left(\mu_l(x-a)\right), \qquad x \in [a,b], \quad \forall\, U(x) \in Y_0,$$

$$\left(P_M^{\mathcal{F}}(U)\right)(x) = \sum_{l=-M/2}^{M/2-1} \widehat{(U)}_l^{\mathcal{F}} \exp\left(i\lambda_l\,(x-a)\right), \qquad x \in [a,b], \quad \forall\, U(x) \in Y_{\rm p},$$

with

$$\widehat{(U)}_l^{\mathcal{S}} = \frac{2}{b-a}\int_a^b U(x)\sin\left(\mu_l(x-a)\right)dx, \qquad l=1,\ldots,M-1, \tag{3.6}$$

$$\widehat{(U)}_l^{\mathcal{F}} = \frac{1}{b-a}\int_a^b U(x)\exp\left(-i\lambda_l\,(x-a)\right)dx, \qquad l=-M/2,\ldots,M/2-1. \tag{3.7}$$

Then for (3.1)-(3.3) with homogeneous Dirichlet boundary conditions (3.4), a backward Euler sine spectral discretization reads:

Find $\phi^{n+1}(x)\in Y_M^{\mathcal{S}}$ (i.e. $\phi^*(x)\in Y_M^{\mathcal{S}}$) such that

$$\frac{\phi^*(x)-\phi^n(x)}{\Delta t} = \frac{1}{2}\partial_{xx}\phi^*(x) - P_M^{\mathcal{S}}\left\{\left[V(x)+C_PV_P^n(x)-\alpha|\phi^n(x)|^{\frac{2}{d}}\right]\phi^*(x)\right\} \tag{3.8}$$

$$\phi^{n+1}(x) = \frac{\phi^*(x)}{\|\phi^*(x)\|_{L^2(a,b)}}, \quad \phi^0(x) = P_M^{\mathcal{S}}\left(\phi_0(x)\right), \quad x\in[a,b], \quad n\geq 0. \tag{3.9}$$

Here, $V_P^n(x)$ is a numerical approximation of the Hartree potential (1.5) at time t_n with $\psi(x,t_n)$ being taken as $\phi^n(x)$, for which the numerical methods will be discussed in the coming subsection.

The above discretization can be solved in phase space but it is not suitable in practice due to the difficulty in computing the integrals in (3.6). In fact, we apply an efficient implementation by choosing $\phi^0(x)$ as the interpolation of $\phi_0(x)$ on the grid points $\{x_j,\, j=0,\ldots M\}$ and approximating the integrals in (3.6) by a numerical quadrature rule on the grid points. Let ϕ_j^n be the approximation of $\phi(x_j,t_n)$ and ϕ^n be a vector with components ϕ_j^n; $(V_P)_j^n$ be the approximation of the Hartree potential $V_P(x_j,t_n)$ from ϕ^n and V_P^n be a vector with components $(V_P)_j^n$. Choosing $\phi_j^0=\phi_0(x_j)$, then for $n=0,1,\ldots$, a backward Euler sine pseudospectral discretization for (3.1)-(3.3) with homogeneous Dirichlet boundary conditions (3.4) reads:

$$\frac{\phi_j^*-\phi_j^n}{\Delta t} = \frac{1}{2}\,D_{xx}^{\mathcal{S}}\phi^*|_{x_j} - \left[V(x_j)+C_P(V_P)_j^n-\alpha|\phi_j^n|^{\frac{2}{d}}\right]\phi_j^*,\ j=1,\ldots,M-1, \tag{3.10}$$

$$\phi_0^*=\phi_M^*=0, \quad \phi_j^{n+1}=\frac{\phi_j^*}{\|\phi^*\|_h}, \quad j=1,\ldots,M-1. \tag{3.11}$$

Here, $D_{xx}^{\mathcal{S}}$ is the sine pseudospectral approximation of ∂_{xx}, defined as

$$D_{xx}^{\mathcal{S}}U|_{x_j} = -\sum_{l=1}^{M-1}(\mu_l)^2\widetilde{(U)}_l^{\mathcal{S}}\sin\left(\mu_l(x_j-a)\right), \quad j=1,2,\ldots,M-1,$$

with $\widetilde{(U)}_l^{\mathcal{S}}$ the discrete sine transform coefficients of the vector $U=(U_0,U_1,\ldots,U_M)^T$ satisfying $U_0=U_M=0$,

$$\widetilde{(U)}_l^{\mathcal{S}} = \frac{2}{M}\sum_{j=1}^{M-1}U_j\sin\left(\mu_l(x_j-a)\right), \qquad l=1,\ldots,M-1.$$

The discrete l^2-norm is defined in standard way, $\|U\|_h^2 = h\sum_{j=0}^{M-1}|U_j|^2$.

The nonlinear system (3.10)-(3.11) can be iteratively solved in phase space efficiently with the help of fast sine transform (FST). The procedure is similar as in [6] and we omit the details here for brevity.

For the problem (3.1)-(3.3) with periodic boundary conditions (3.5), with a similar procedure as above a backward Euler Fourier spectral discretization can be proposed, i.e., replacing $Y_M^{\mathcal{S}}$ and $P_M^{\mathcal{S}}$ in (3.8)-(3.9) by $Y_M^{\mathcal{F}}$ and $P_M^{\mathcal{F}}$ respectively. Similarly, a practical implementation, a backward Euler Fourier pseudospectral discretization, will be used in computation which is similar as (3.10)-(3.11) but defined on proper index set, replacing $D_{xx}^{\mathcal{S}}$ by the Fourier pseudospectral approximation of ∂_{xx}, defined as

$$D_{xx}^{\mathcal{F}} U|_{x_j} = -\sum_{l=-M/2}^{M/2-1} (\lambda_l)^2 \widetilde{(U)}_l^{\mathcal{F}} \exp\left(i\lambda_l\left(x_j-a\right)\right), \quad j=0,1,\ldots,M-1,$$

with $\widetilde{(U)}_l^{\mathcal{F}}$ the discrete Fourier transform coefficients of the vector $U=(U_0,U_1,\ldots,U_M)^T$ satisfying $U_0=U_M$,

$$\widetilde{(U)}_l^{\mathcal{F}} = \frac{1}{M}\sum_{j=0}^{M-1} U_j \exp\left(-i\lambda_l\left(x_j-a\right)\right), \qquad l=-M/2,\ldots,M/2-1.$$

The backward Euler Fourier pseudospectral discretization can also be iteratively solved in phase space efficiently with the help of FFT.

3.2. Methods for computing Hartree potential

In this subsection, we propose different ways to obtain the approximations $(V_P)_j^n$ from the vector ϕ^n. The methods we propose here include fast convolution, sine pseudospectral and Fourier pseudospectral approaches.

Fast convolution method is the approach to approximate the convolution (1.5) on grid points with fast algorithms. Since the convolution kernel changes with the dimension of space, the algorithms also vary in different dimensions.

In 1D, we first consider the problem (3.1)-(3.3) with homogeneous Dirichlet boundary conditions (3.4). For $n\geq 0$ with $\rho^n := \left(|\phi_0^n|^2,|\phi_1^n|^2,\ldots,|\phi_M^n|^2\right)^T$ the Hartree potential approximation $(V_P)_j^n$ in (3.10) is obtained by

$$(V_P)_j^n = -\frac{1}{2}\sum_{l=1}^{M-1} \widetilde{(\rho^n)}_l^{\mathcal{S}} \int_a^b |x_j-y|\sin\left(\mu_l(y-a)\right)dy, \qquad j=1,\ldots,M-1. \tag{3.12}$$

The integrals in above can be evaluated exactly since

$$\begin{aligned}\int_a^b |x-y|\sin\left(\mu_l(y-a)\right)dy &= \frac{1}{\mu_l}\left[(1+(-1)^l)x-(a+(-1)^l b)\right]\\ &\quad -\frac{2}{(\mu_l)^2}\sin\left(\mu_l(x-a)\right), \qquad x\in[a,b], \quad l=1,\ldots,M-1.\end{aligned} \tag{3.13}$$

Thus,

$$\begin{aligned}(V_P)_j^n &= \sum_{l=1}^{M-1} \widetilde{(\rho^n)}_l^{\mathcal{S}} \frac{a+(-1)^l b}{2\mu_l} - x_j\cdot\sum_{l=1}^{M-1} \widetilde{(\rho^n)}_l^{\mathcal{S}} \frac{1+(-1)^l}{2\mu_l}\\ &\quad + \sum_{l=1}^{M-1} \frac{\widetilde{(\rho^n)}_l^{\mathcal{S}}}{(\mu_l)^2}\sin\left(\mu_l(x_j-a)\right) := S_1 - x_j\cdot S_2 + S_3, \quad j=1,\ldots,M-1.\end{aligned} \tag{3.14}$$

Since the summation terms S_1 and S_2 are uniform for any $j = 1, \ldots, M-1$ and S_3 can be evaluated efficiently with the help of FST, the overall computation cost reduces from $O(M^2)$ for direct convolution to $O(M \ln(M))$. Hereafter we refer the fast algorithm (3.14) as 1D fast convolution method in homogeneous Dirichlet boundary conditions case. Combining this 1D fast convolution method with (3.10)-(3.11), we are lead to a backward Euler sine pseudospectral+fast convolution (BSFC) discretization to compute the ground state in 1D. On the other hand, for the 1D problem (3.1)-(3.3) with periodic boundary conditions (3.5), a similar fast convolution algorithm can also be achieved with the help of FFT and noting

$$\int_a^b |x-y| \exp\left(i\lambda_l (y-a)\right) dy$$
$$= \begin{cases} \dfrac{2}{(\lambda_l)^2}\left[1 - \exp\left(i\lambda_l (x-a)\right)\right] + \dfrac{(a+b-2x)}{i\lambda_l}, & l = -\dfrac{M}{2}, \ldots, -1, 1, \ldots, \dfrac{M}{2} - 1, \\ x^2 - (a+b)x + \dfrac{a^2+b^2}{2}, & l = 0, \end{cases}$$

which combines with the backward Euler Fourier pseudospectral discretization (BFFC) to compute the ground state in 1D with periodic boundary conditions.

In higher dimensions, i.e. $d = 2$ and 3, the above fast algorithms cannot be generalized since there is no analytical formula to evaluate the convolution of $G_d(|\mathbf{x}|)$ with sine or Fourier base functions. In what follows, the 2D and 3D convolution are accelerated by fast multipole method (FMM), for which the computational cost is $O(N)$ with N being the number of target points (grid points). Backward Euler sine/Fourier pseudospectral discretization combined with such fast convolution approximation (BSFC/BFFC) is used to compute the 2D or 3D ground state, depending on the boundary conditions made on the wave function.

For simplicity of notations, we assume the domain Ω to be a square and a cube in 2D and 3D respectively, i.e. $\Omega^2 := [a,b] \times [a,b]$ and $\Omega^3 := [a,b] \times [a,b] \times [a,b]$, and grid points in y-axis and z-axis to be $y_k = a + kh$ and $z_l = a + lh$ for $k, l = 0, 1, \ldots, M$. Given $\phi_{jk}^n \approx \phi(x_j, y_k, t_n)$ and $\phi_{jkl}^n \approx \phi(x_j, y_k, z_l, t_n)$, we first interpolate the density function $\rho(\mathbf{x}, t_n) := |\phi(\mathbf{x}, t_n)|^2$ by a piecewise bilinear and trilinear function $\rho_h^n(\mathbf{x})$ in 2D and 3D respectively. Then, $(V_P)_{jk}^n \approx V_P(x_j, y_k, t_n)$, and $(V_P)_{jkl}^n \approx V_P(x_j, y_k, z_l, t_n)$ are obtained by evaluating

$$-\frac{1}{2\pi}\int_{\Omega^2} \ln\left(|\mathbf{x}-\mathbf{y}|\right) \rho_h^n(\mathbf{y}) d\mathbf{y}, \quad \text{and} \quad \frac{1}{4\pi}\int_{\Omega^3} \frac{1}{|\mathbf{x}-\mathbf{y}|} \rho_h^n(\mathbf{y}) d\mathbf{y}, \tag{3.15}$$

at target points.

In order to calculate the above convolution efficiently, FMM is applied by following [24] for 2D and [19, 26, 42] for 3D. Here we shall only sketch the procedure. First, an oct-tree hierarchy is imposed on Ω^3 by dividing the cube into eight sub cubes recursively. Similarly, a quad-tree is superimposed on Ω^2 in 2D. We refer the readers to [24, 25, 26] for detailed tree structures and their adaptivity. In FMM, the far field interactions are calculated by means of multipole expansions (via upward pass) and it converts the multipole expansions into local expansions (via downward pass) relying on three kind of translation operators acting on multipole and local expansions in the tree hierarchy: multipole-to-multipole ($\mathcal{T}_{MM}$), multipole-to-local ($\mathcal{T}_{ML}$), and local-to-local ($\mathcal{T}_{LL}$) translations. Last, direct interactions (influence from neighbors of a leaf node and itself) are computed according to (3.15). We omit the algorithms here for brevity and refer to [19, 24, 26] for the technical details. The

most time-consuming translation operator $\mathcal{T}_{ML}$ is accelerated by plane wave method as described in [28, 19] for 2D and 3D. To calculate the integrals in the multipole and local expansions efficiently, recurrence formulas for the spherical harmonics are helpful (refer to [41]). For regular integral in (3.15), Gaussian quadrature is applied. In our implementation, both multipole and local expansions are truncated to $p = 18$ terms which allows a 6-digits precision.

Sine pseudospectral approximation is the approach to solve the Poisson equation (1.2) (or its modified equation) on the bounded domain Ω with homogeneous Dirichlet boundary conditions by using sine pseudospectral method. In 1D, we consider the problem (3.1)-(3.3) with homogeneous Dirichlet boundary conditions (3.4) and at each time t_n, given ϕ^n consider the following problem

$$\partial_{xx} V_P(x_j, t_n) = -|\phi_j^n|^2, \qquad j = 1, \ldots, M-1, \qquad n \geq 0 \tag{3.16}$$

$$V_P(x_0, t_n) = (V_P)_0^n, \qquad V_P(x_M, t_n) = (V_P)_M^n, \tag{3.17}$$

where, $(V_P)_0^n$ and $(V_P)_M^n$ are two approximated boundary conditions which, for example, can be obtained from (3.14) by letting $j = 0$ and M respectively. Then a sine pseudospectral discretization to a modified problem of (3.16)-(3.17) reads

$$D_{xx}^{\mathcal{S}} V_P^*(x, t_n)|_{x_j} = -|\phi_j^n|^2, \qquad j = 1, \ldots, M-1, \qquad n \geq 0 \tag{3.18}$$

$$V_P^*(x_0, t_n) = V_P^*(x_M, t_n) = 0, \tag{3.19}$$

where

$$V_P^*(x, t) = V_P(x, t) - \frac{(V_P)_M^n - (V_P)_0^n}{b-a}(x-a) - (V_P)_0^n. \tag{3.20}$$

Solving (3.18)-(3.19) in phase space, we obtain for $j = 1, \ldots, M-1$

$$(V_P)_j^n = \sum_{l=1}^{M-1} \frac{\widetilde{(\rho^n)}_l^{\mathcal{S}}}{(\mu_l)^2} \sin\left(\mu_l (x_j - a)\right) + \frac{(V_P)_M^n - (V_P)_0^n}{b-a}(x_j - a) + (V_P)_0^n. \tag{3.21}$$

Note that if the external potential $V_{\text{ext}}(x)$ is symmetric, without loss of generality $V_{\text{ext}}(x)$ is an even function, then the solution of (2.6)-(2.8) $\phi(x, t)$ should also be even. Therefore, it is reasonable to choose $a = -b$ and the approximated boundary conditions $(V_P)_0^n = (V_P)_M^n = 0$ in (3.18)-(3.19) due to (1.5). Then, the approximation in (3.21) is just a constant translation of the result by applying the sine pseudospectral discretization to (3.16) with $(V_P)_0^n = (V_P)_M^n = 0$. In the view of any constant translation of external potential will leave the ground state unchanged, we can simply choose $(V_P)_0^n = (V_P)_M^n = 0$ when $V_{\text{ext}}(x)$ is an even function, i.e. the Hartree potential is approximated by

$$(V_P)_j^n = \sum_{l=1}^{M-1} \frac{\widetilde{(\rho^n)}_l^{\mathcal{S}}}{(\mu_l)^2} \sin\left(\mu_l (x_j - a)\right), \qquad j = 1, \ldots, M-1. \tag{3.22}$$

In 3D, the far-field condition of $V_P(\mathbf{x}, t)$ being $\lim_{|\mathbf{x}|\to\infty} |V_P(\mathbf{x}, t)| = 0$ can be drawn from (1.5), and therefore the sine pseudospectral discretization in 3D is a straightforward generalization of (3.22) by tensor product grids without any modification provided that the bounded domain Ω is chosen large enough.

Hereafter, we refer (3.21) or (3.22) for an even external potential, and the generalization of (3.22) in 3D as sine pseudospectral approximation of (1.5). Combining this method with (3.10)-(3.11), we obtain a backward Euler sine pseudospectral (BESP) discretization to compute the ground state in $d = 1$, 3 space dimensions.

Remark 3.1. *In 2D, to obtain appropriate approximated boundary conditions with high-order of accuracy is a costly job itself. Meanwhile, no homogenization tool like (3.18)-(3.20) is available in general for 2D problems. Thus, the homogeneous boundary conditions cannot be satisfied, and the sine pseudospectral approach is not applicable in 2D. Here, we remark that the work to propose a spectral-type approach in 2D is still on-going.*

Fourier pseudospectral approximation is the approach to solve the Poisson equation (1.2) (or its modified equation) on the bounded domain Ω with periodic boundary conditions by using Fourier pseudospectral method. In 1D, we consider the problem (3.1)-(3.3) with periodic boundary conditions (3.5). At each time t_n, for (3.16)-(3.17) and introducing

$$V_P^*(x,t) = V_P(x,t) - \frac{(V_P)_M^n - (V_P)_0^n}{b-a}(x-a), \tag{3.23}$$

we get a modified problem

$$\partial_{xx} V_P^*(x_j,t_n) = -|\phi_j^n|^2, \qquad j = 0,\dots,M-1, \qquad n \geq 0 \tag{3.24}$$

$$V_P^*(x_0,t_n) = V_P^*(x_M,t_n), \tag{3.25}$$

which determines a unique V_P^* up to a constant translation. A Fourier pseudospectral discretization applying to the modified problem (3.24)-(3.25) reads

$$D_{xx}^{\mathcal{F}} V_P^*(x,t_n)|_{x_j} = -|\phi_j^n|^2 + \frac{1}{b-a}, \qquad j = 0,\dots,M-1, \qquad n \geq 0 \tag{3.26}$$

$$V_P^*(x_0,t_n) = V_P^*(x_M,t_n). \tag{3.27}$$

Adding the last term in (3.26) is due to the consistency requirement in 0-mode after taking Fourier transform on both sides of (3.24) and the normalization condition of ϕ^n. Then $(V_P^n)_j$ for $j = 0,1,\dots,M-1$ is obtained by

$$(V_P)_j^n = \sum_{l=-M/2}^{M/2-1} \widetilde{(V_P^*)}_l^{\mathcal{F}} \exp\left(i\lambda_l (x_j - a)\right) + \frac{(V_P)_M^n - (V_P)_0^n}{b-a}(x_j - a), \tag{3.28}$$

where $\widetilde{(V_P^*)}_l^{\mathcal{F}} = \dfrac{\widetilde{(\rho^n)}_l^{\mathcal{F}}}{(\mu_l)^2}$ for $l \neq 0$, and usually we choose $\widetilde{(V_P^*)}_0^{\mathcal{F}} = 0$. In fact, $\widetilde{(V_P^*)}_0^{\mathcal{F}}$ can be chosen as any value since any constant translation of potential leaves the ground state unchanged.

We remark here that although the above approximation is expected to have a spectral order of accuracy, the error from adding $(b-a)^{-1}$ in (3.26) to ensure the consistency in 0-mode will dominate. It implies that the approximation will converge as $b-a$ becomes larger, as shown in the above method derivation and the numerical results reported in the next section. Therefore, in practice if periodic boundary conditions are of interests and the Fourier approach is applied, a large computation domain is necessary. However, it is noted that the Fourier approach for solving (3.26)-(3.27) is spectrally accurate as numerically shown in the next section, so with only a few grid points it can already achieve the conserved approximation with respect to the computation domain. On the other hand, it can be implemented very efficiently thanks to FFT. Thus, to obtain a good approximation one can implement it on a large computation domain but with relatively few grid points,

and the computation cost would be much less than other discretization methods, like finite difference or finite element approaches.

Similar as the sine pseudospectral discretization, in 1D if the external potential $V_{\rm ext}(x)$ is an even function, then $(V_P^n)_j$ can be simply evaluated by

$$(V_P)_j^n = \sum_{l=-M/2}^{M/2-1} \widetilde{\left(V_P^*\right)}_l^{\mathcal{F}} \exp\left(i\lambda_l\left(x_j - a\right)\right), \tag{3.29}$$

provided $a = -b$. Again, the Fourier pseudospectral discretization in 3D is a straightforward generalization of (3.29) with tensor product grids, while such discretization is not suitable to 2D case for similar reasons as pointed out in Remark 3.1. With such approximation it leads to a backward Euler Fourier pseudospectral (BEFP) discretization for computing the ground state in $d = 1$, 3 space dimensions.

Remark 3.2. *If the external potential $V_{\rm ext}$ is radially symmetric in 2D or spherically symmetric in 3D, then it is known that the ground state has the same type of symmetry. In these two cases, the original problem collapses to a quasi-1D problem (similar as [7, Appendix A.1]), where the operator Δ collapses to $r^{1-d}\partial_r\left(r^{d-1}\partial_r\right)$ with $r = |\mathbf{x}|$ and $d = 2$, 3. In the quasi-1D problem, $\phi(r)$ is with homogeneous Dirichlet boundary conditions and Hartree potential V_P is with Robin boundary conditions. In the view of the spatial derivative operator and the boundary conditions, the above spectral methods based on sine or Fourier base functions cannot be directly extended, and we suggest to apply the standard finite difference discretization in space followed by the proposed backward Euler integration in time to compute the ground state with radial or spherical symmetry.*

4. Numerical methods for computing dynamics

In this section, we present an efficient and accurate time-splitting sine or Fourier pseudospectral discretization, coupled with the various approaches proposed in Section 3.2 for approximating the Hartree potential, to compute the dynamics of the SPS system (1.1)-(1.3) or (1.4).

Again, in practice the whole space problem is truncated into a bounded computation domain Ω with either homogeneous Dirichlet or periodic boundary conditions. For simplicity of notations, we shall introduce the discretization in 1D with homogeneous Dirichlet boundary conditions. Generalizations to higher space dimensions or periodic boundary conditions proceed in the same manner as in the last section. In 1D, from $t = t_n$ to $t = t_{n+1}$, the problem (1.4) on $\Omega = [a, b]$ with homogeneous Dirichlet boundary conditions splits into two steps. One solves first the free Schrödinger equation

$$i\,\partial_t\psi(x,t) = -\frac{1}{2}\partial_{xx}\psi(x,t), \qquad \psi(a,t) = \psi(b,t) = 0, \qquad t_n \le t \le t_{n+1}, \tag{4.1}$$

for the time step with length Δt, followed by solving

$$i\,\partial_t\psi(x,t) = \left[V_{\rm ext}(x) + C_P V_P\left(|\psi|^2\right) - \alpha|\psi|^2\right]\psi, \quad t_n \le t \le t_{n+1}, \tag{4.2}$$

for the same time step. Similar as [9, 10] the problem (4.1) is discretized in space by sine pseudospectral method and integrated in phase space exactly. For $t_n \le t \le t_{n+1}$, (4.2) leaves $|\psi|$ (so as V_P) unchanged in t and thus it collapse to

$$i\,\partial_t\psi(x,t) = \left[V_{\rm ext}(x) + C_P V_P\left(|\psi(x,t_n)|^2\right) - \alpha|\psi(x,t_n)|^2\right]\psi, \quad t_n \le t \le t_{n+1}, \tag{4.3}$$

The linear ODE (4.3) is integrated in time exactly with the Hartree potential V_P being approximated by methods proposed in Section 3.2. Let ψ_j^n be the approximation of $\psi(x_j, t_n)$ and ψ^n be the approximation vector with components ψ_j^n; $(V_P)_j^n$ be the approximation of the Hartree potential $V_P(x_j, t_n)$ from ψ^n and V_P^n be a vector with components $(V_P)_j^n$; and choose $\psi_j^0 = \psi_0(x_j)$ for $j = 0, \ldots, M$. For $n = 0, 1, \ldots$, a detailed second order time-splitting sine pseudospectral discretization via Strang formula [9, 10, 39], applied in our computing, is as follows

$$\psi_j^* = \sum_{l=1}^{M-1} \exp\left(-i\Delta t \mu_l^2/4\right) \widetilde{(\psi^n)}_l^{\mathcal{S}} \sin\left(\mu_l(x_j - a)\right), \tag{4.4}$$

$$\psi_j^{**} = \exp\left[-i\Delta t \left(V(x_j) + C_P(V_P^*)_j - \alpha|\psi_j^*|^2\right)\right] \psi_j^*, \tag{4.5}$$

$$\psi_j^{n+1} = \sum_{l=1}^{M-1} \exp\left(-i\Delta t \mu_l^2/4\right) \widetilde{(\psi^{**})}_l^{\mathcal{S}} \sin\left(\mu_l(x_j - a)\right), \tag{4.6}$$

for $j = 1, \ldots, M-1$. Here, $\widetilde{(\psi^n)}_l^{\mathcal{S}}$ is the discrete sine transform coefficients of ψ^n. Evaluating $(V_P^*)_j$ via sine pseudospectral method (3.21) leads to a time-splitting sine pseudospectral (TSSP) discretization to compute the dynamics. Similarly, a time-splitting sine pseudospectral+fast convolution (TSFC) method is obtained by evaluating $(V_P^*)_j$ via the fast convolution approach (3.14). These methods are explicit, unconditionally stable and time reversible. In fact, for the stability, we have

Lemma 4.1. *TSFC and TSSP are normalization conserved, i.e.*

$$\|\psi^n\|_h^2 := h \sum_{j=0}^{M-1} \left|\psi_j^n\right|^2 \equiv h \sum_{j=0}^{M-1} \left|\psi_j^0\right|^2 = \left\|\psi^0\right\|_h^2, \qquad n \geq 0. \tag{4.7}$$

Proof: The argument process in analogous lines as in [9, 10] and we omit the details here for brevity. □

In periodic boundary conditions case, a similar time-splitting Fourier pseudospectral discretization can be proposed. It combines with Fourier pseudospectral method (3.28), i.e., TSFP, or with fast convolution approach based on Fourier bases, i.e. TFFC, to compute the dynamics. We omit the details here for brevity. Also, they are explicit, time reversible, time traversable and unconditionally stable.

Note that in the special case that the external potential is even, then $(V_P^*)_j$ can be again simply obtained by (3.22) or (3.29). This is because from t_n to t_{n+1}, if a constant c is added to potential $(V_P^*)_j$, then ψ_j^{n+1} obtained from time-splitting sine or Fourier pseudospectral approaches get multiplied by a phase factor $\exp(-i\Delta t C_P \cdot c)$, which leaves $|\psi_j^{n+1}|$ unchanged and so as for any discrete quadratic observables, for example the particle density $\rho_j^n = |\psi_j^n|^2$, and such observables are of real interests in application.

Remark 4.1. *If the external potential V_{ext} and the initial condition ψ_0 are both radically symmetric in 2D or spherically symmetric in 3D, then the original problem collapses to a quasi-1D problem. For similar reasons as pointed out in Remark 3.2, in these two cases the above spectral methods cannot be directly extended, and we suggest to use a Crank-Nicolson finite difference [23, 27] discretization to compute the dynamics.*

Table 1: Ground state error analysis in Example 1. (1) $\|\phi_g - \phi_{g,h}\|_\infty$ versus mesh size h on $\Omega = [-16, 16]$ for BSFC, BESP and BEFP (upper part); (2) $\|\phi_g - \phi_{g,h}\|_\infty$ versus bounded domain $\Omega = [-a, a]$ with $h = 1/16$ for BEFP (last row).

mesh size	$h = 1$	$h = 1/2$	$h = 1/4$	$h = 1/8$	$h = 1/16$
BSFC	7.644E-03	4.076E-06	1.400E-12	<E-12	<E-12
BESP	7.644E-03	4.076E-06	1.400E-12	<E-12	<E-12
BEFP	5.725E-03	1.074E-02	1.074E-02	1.074E-02	1.074E-0
domain	$a = 8$	$a = 16$	$a = 32$	$a = 64$	$a = 128$
BEFP	2.297E-02	1.078E-02	5.235E-03	2.581E-03	1.281E-03

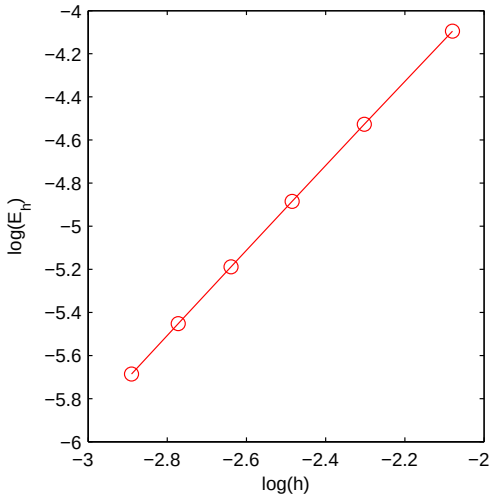

Figure 1: Ground state error analysis in Example 2. Plot of $\log(\|\phi_g - \phi_{g,h}\|_\infty)$ versus $\log(h)$ for 3D BSFC method on a cube $[-4, 4]^3$ with uniform grids in each axis.

5. Numerical results

In this section, extensive numerical experiment results on computing the ground states and dynamics of the SPS system (1.1)-(1.3) are reported. In what follows, we begin with the comparisons of different methods proposed before and then apply the methods BESP and TSSP to 3D SPS system in various setups

5.1. Comparison of different methods for ground state

In order to reflect the effects of different Hartree potential approximations on the computed ground states, we only present the results for the most simplest form of (1.1)-(1.3), i.e., the SN system.

Example 1. Ground state of 1D SN system without external potential, i.e., $d = 1$, $V_{\text{ext}} = 0$, $C_P < 0$ and $\alpha = 0$ in (1.1), and we choose $C_P = -3$. In our computation, we choose the initial guess as $\phi_0 = \frac{1}{\pi^{1/4}} e^{-\frac{1}{2}x^2}$, $x \in \mathbb{R}$, and use time step $k = 0.005$. Let ϕ_g be the "exact" ground state obtained from BSFC with a very fine mesh size $h = 1/128$ on $\Omega = [-128, 128]$. $\phi_{g,h}$ denotes the approximated ground state obtained from different methods with mesh

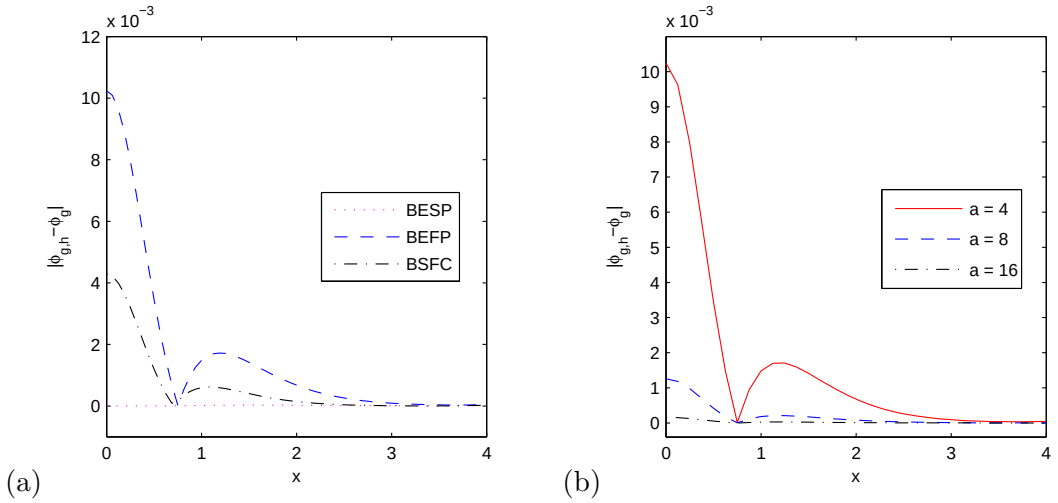

Figure 2: Ground state error analysis in Example 2. (a) Slice plots of $|\phi_g - \phi_{g,h}|$ along x-axis for 3D BSFC, BESP and BEFP in cube $[-4,4]^3$ with uniform mesh size $h = 1/16$ in each axis; (b) slice plots of $|\phi_g - \phi_{g,h}|$ along x-axis for BEFP in different cubes $[-a,a]^3$ with uniform mesh size $h = 1/8$ in each axis.

size h. Tab. 1 shows the errors $\|\phi_g - \phi_{g,h}\|_\infty$ of the methods BSFC, BESP and BEFP on $\Omega = [-16,16]$ for various mesh sizes h and $\|\phi_g - \phi_{g,h}\|_\infty$ of BEFP on different domains Ω with $h = 1/16$.

Example 2. Ground state of 3D SN system without external potential, i.e.,$d = 3$, $V_{\text{ext}} = 0$, $C_P < 0$ and $\alpha = 0$ in (1.1), and we choose $C_P = -75$. In our computation, the initial guess is chosen as $\phi_0 = \frac{1}{(6\pi)^{3/4}} e^{-\frac{x^2+y^2+z^2}{12}}$, $(x,y,z) \in \mathbb{R}^3$, and time step is $k = 0.01$. Since the ground state of this SN system is radially symmetric, a benchmark is achieved by using a Backward Euler finite difference method to the reduced quasi-1D model of GFDN (2.6)-(2.8) with Dirichlet boundary conditions of ϕ and Robin boundary conditions of V_P. The "exact" solution $\phi(r)$ is computed in a ball $0 \le r \le 8$ with a very fine mesh size $\Delta r = 1/1024$. Fig. 1 shows the convergence rate of BSFC method in 3D, which applies FMM to accelerate the direct convolution (1.5). Fig. 2 depicts the slice plots of error $|\phi_g - \phi_{g,h}|$ along x-axis for 3D BSFC, BESP and BEFP methods in a cube $[-4,4]^3$ with uniform mesh size $h = 1/16$ in each axis, and for BEFP in different cubes with uniform mesh size $h = 1/8$ in each axis.

From Tab. 1, Fig. 1, 2 and additional results not shown here, the following observations are made:

(i). BESP and 1D BSFC methods both have spectral order of accuracy (cf. Tab. 1), and 2D and 3D BSFC methods have second-order of accuracy in spatial discretization (cf. Fig. 1).

(ii). For BEFP method, the error from the truncated computation domain dominates and it has a low order of accuracy instead of spectral order of accuracy expected for spectral-type method. This is observed in the error $\|\phi_g - \phi_{g,h}\|_\infty$ versus h of BEFP for a fixed domain (cf. the 3rd row in Tab. 1), which remains to be a uniform bound when h goes to finer. In addition, as indicated by the formulation of method, the approximated ground state will converge as the truncated domain is chosen larger (cf. the last row in Tab. 1 and (b) in Fig. 2).

(iii). In 3D, BEFP method is a better choice than BSFC method which applies FMM to accelerate the convolution. Comparing (a) and (b) in Fig. 2 (cf. "$- \cdot - \cdot -$" in (a) versus

Table 2: Density error analysis in Example 3. (1) $\|\rho - \rho_h\|_\infty$ at $t = 1.0$ versus mesh size h on $\Omega = [-16, 16]$ for TSFC, TSSP and TSFP (upper part); (2) $\|\rho - \rho_h\|_\infty$ at $t = 1.0$ versus bounded domain $\Omega = [-a, a]$ with $h = 1/32$ for BEFP (last row).

mesh size	$h = 1$	$h = 1/2$	$h = 1/4$	$h = 1/8$	$h = 1/16$
TSFC	5.017E-02	1.531E-02	1.120E-05	1.412E-12	<E-12
TSSP	5.017E-02	1.531E-02	1.120E-05	1.396E-12	<E-12
TSFP	5.412E-02	3.968E-02	2.345E-02	2.345E-02	2.345E-02
domain	$a = 8$	$a = 16$	$a = 32$	$a = 64$	$a = 128$
TSFP	6.207E-02	2.345E-02	1.107E-02	5.395E-03	2.654E-03

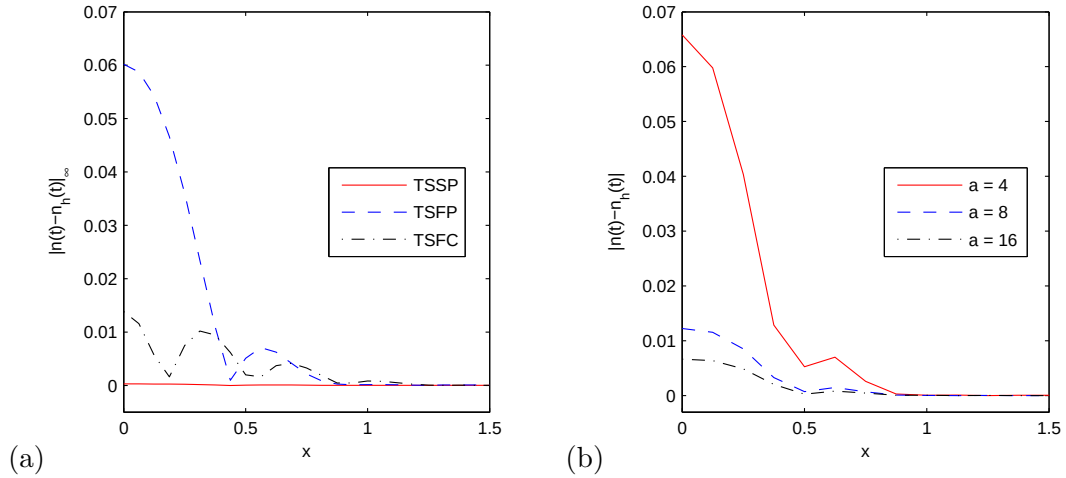

Figure 3: Density error analysis in Example 4. (a) Slice plots of $|\rho - \rho_h|$ along x-axis for 3D TSFC, TSSP and TSFP in a cube $[-4, 4]^3$ with uniform mesh size $h = 1/16$ in each axis; (b) slice plots of $|\rho - \rho_h|$ along x-axis for TSFP in different cubes $[-a, a]^3$ with uniform mesh size $h = 1/8$ in each axis.

"– – – –" in (b)), it shows that with the same number of grid points, BEFP method gives better approximations than BSFC method. In addition, the implementation of BEFP is much more efficient due to FFT.

(iv). In the view of both efficiency and accuracy, BESP method is the best choice for computing the ground state of the SPS system in 3D.

5.2. Comparison of different methods for dynamics

Again, we carry out the comparisons for the SN system in 1D and 3D.

Example 3. Dynamics of 1D SN system without external potential, i.e., $d = 1$, $V_{\text{ext}} = 0$, $C_P < 0$ and $\alpha = 0$ in (1.1), and we choose $C_P = -20$. The initial value is taken as $\psi_0(\mathbf{x}) = \frac{1}{\pi^{1/4}} e^{-x^2/2}$, $x \in \mathbb{R}$. Here we focus on the spatial resolution capacity of different methods, and hence we fix a very small time step $k = 0.0001$ such that the error from time discretization is negligible. The "exact" solution of wave function ψ and density $\rho = |\psi|^2$ are computed from TSFC on $\Omega = [-64, 64]$ with a very fine mesh size $h = 1/32$. $\rho_h = |\psi_h|^2$ denotes the approximated density with mesh size h. Tab. 2 shows the density errors

Table 3: Different quantities in the ground state of SPS system for Poisson coefficient $C_P = 1$ with different exchange coefficients α under $V_{\text{ext}} = \frac{1}{2}\left(x^2 + y^2 + 4z^2\right)$.

α	E^g_{kin}	E^g_{pot}	E^g_{int}	E^g_{exc}	E^g	μ^g	σ^g_x	σ^g_z	$\rho_g(0)$
0.1	0.999	1.001	0.031	-0.031	2.000	2.021	0.501	0.250	0.503
0.5	1.031	0.970	0.032	-0.157	1.876	1.855	0.481	0.245	0.519
1	1.074	0.932	0.032	-0.321	1.717	1.642	0.455	0.238	0.540
5	1.619	0.635	0.038	-2.013	0.279	-0.355	0.272	0.182	0.786
10	3.154	0.348	0.057	-5.677	-2.118	-3.953	0.128	0.110	1.357

$\|\rho(t) - \rho_h(t)\|_\infty$ at $t = 1.0$ of the methods TSFC, TSSP and TSFP with different mesh sizes h on $\Omega = [-16, 16]$, and the similar error of TSFP on different domains Ω with $h = 1/32$.

Example 4. Dynamics of 3D SN system without external potential, i.e., $d = 3$, $V_{\text{ext}} = 0$, $C_P < 0$ and $\alpha = 0$ in (1.1) and we choose $C_P = -200$. A radially symmetric initial value is chosen as $\psi_0 = \frac{1}{(\pi/2)^{\frac{3}{4}}} e^{-(x^2+y^2+z^2)}$. A benchmark is obtained by applying a Crank-Nicolson finite difference method to the reduced 1D model due to the radial symmetry property. The "exact" solution $\psi(r, t)$, is computed in a ball $0 \le r \le 8$ with a very fine mesh size $\Delta r = 1/1024$ and a very fine time step $\Delta t = 0.00001$. TSFC, TSSP and TSFP methods are compared with the same time step $k = 0.001$. Slice plots of $|\rho - \rho_h|$ along x-axis of these methods in a cube $[-4, 4]^3$ with uniform mesh size $h = 1/16$ in each axis, and for TSFP in different cubes with uniform mesh size $h = 1/8$ in each axis are shown in Fig. 3.

From Tab. 2, Fig. 3 and additional results not shown here, similar conclusions about the convergence in spatial discretization for TSFC, TSSP and TSFP methods can be drawn, as those made after Example 1 and 2. Also, TSSP method is the best choice for computing the dynamics of the SPS system in 3D.

5.3. Application

In this subsection, we apply the BESP and TSSP methods to compute the ground states and dynamics of 3D SPS system with different sets of parameters as well as under various types of external potential.

Example 5. Ground states of 3D SPS in different setups. We are interested in the following three cases:

CASE I: fixed Poisson potential coefficient, e.g., $C_P = 1$, with different exchange coefficients α. Here we consider the system under a trapping potential $V_{\text{ext}} = \frac{1}{2}\left(x^2 + y^2 + 4z^2\right)$. Tab. 3 lists different quantities in the ground state for this case, which shows that for a fixed Poisson constant C_P, when α increases, the energy E^g, chemical energy μ^g, potential energy E^g_{pot}, exchange energy E^g_{exc}, condensate widths σ^g_x and σ^g_z decrease, and the kinetic energy E^g_{kin}, interaction energy E^g_{int} and central density $\rho^g(0)$ increase.

CASE II: different Poisson potential coefficients C_P without exchange term under a trapping potential $V_{\text{ext}} = \frac{1}{2}\left(x^2 + y^2 + 4z^2\right)$. Different quantities in the ground state for this case are listed in Tab. 4, which shows that without exchange effect, i.e. $\alpha = 0$, when the Poisson constant C_P increases from negative (attractive) to positive (repulsive), the energy E^g, chemical energy μ^g, potential energy E^g_{pot} and interaction energy E^g_{int} increase, and the kinetic energy E^g_{kin}, and central density $\rho^g(0)$ decrease.

Table 4: Different quantities in the ground state of SPS system without exchange term for different Poisson coefficients C_P under $V_{\rm ext} = \frac{1}{2}\left(x^2+y^2+z^2\right)$.

C_P	$E^g_{\rm kin}$	$E^g_{\rm pot}$	$E^g_{\rm int}$	$E^g_{\rm exc}$	E^g	μ^g	$\rho_g(0)$
-50	1.516	0.377	-1.845	0.000	0.048	-1.797	0.780
-10	0.839	0.671	-0.293	0.000	1.217	0.923	0.471
-5	0.792	0.710	-0.142	0.000	1.361	1.219	0.446
0	0.750	0.750	0.000	0.000	1.500	1.500	0.424
5	0.713	0.790	0.111	0.000	1.613	1.724	0.404
10	0.679	0.829	0.258	0.000	1.766	2.023	0.385
50	0.502	1.137	1.054	0.000	2.694	3.748	0.280

CASE III: ground states under various external potentials. Fig. 4 depicts the surface plots of ground state $|\phi_g(x,0,z)|^2$ and isosurface plots of $|\phi_g| = 0.01$ of the SPS system (1.1) with $C_P = 100$, $\alpha = 1$ and under: (1) harmonic potential $V_{\rm ext} = \frac{1}{2}(x^2+y^2+z^2)$; (ii) double-well potential $V_{\rm ext} = \frac{1}{2}(x^2+y^2+z^2) + 4e^{-\frac{1}{2}z^2}$; (iii) optical lattice potential $V_{\rm ext} = \frac{1}{2}(x^2+y^2+z^2) + 20\left[\sin(\pi x)^2 + \sin(\pi y)^2 + \sin(\pi z)^2\right]$.

Example 6. Dynamics of 3D SPS system in different setups. In our computation, the initial data $\psi_0(\mathbf{x})$ is chosen as the ground state computed numerically for $C_P = 1, \alpha = 5, V_{\rm ext} = \frac{1}{2}(x^2+y^2+4z^2)$. First, the slater coefficient is suddenly changed from $\alpha = 5$ to $\alpha = 10$ while keeping all the other parameters unchanged. Fig. 5 depicts the time evolution of total energy $E(t)$, kinetic energy $E_{\rm kin}(t)$, potential energy $E_{\rm pot}(t)$, interaction energy $E_{\rm int}(t)$, exchange energy $E_{\rm exc}(t)$, chemical potential $\mu(t)$, condensate width $\sigma_x(t)$, $\sigma_z(t)$, central density $\rho_0(t) := |\psi(0,0,0,t)|^2$ and the isosurface plots of density $\rho(\mathbf{x},t) := |\psi(\mathbf{x},t)|^2 = 0.01$ at different time points. Next, Fig. 6 shows the similar quantities for the case of suddenly changing the trapping potential from $V_{\rm ext} = \frac{1}{2}(x^2+y^2+4z^2)$ to $V_{\rm ext} = \frac{1}{2}(x^2+y^2+36z^2)$ and keeping all the other parameters unchanged.

In Fig. 5 and 6, a periodic profile of kinetic energy, potential energy, interaction energy, exchange energy, chemical potential, condensate width and density is observed. In addition, the total energy is numerically conserved very well by the TSSP method.

6. Conclusions

In this work we considered the numerics of the Schrödinger-Poisson-Slater (SPS) system in all space dimensions. To compute the ground state and dynamics of the SPS system, a backward Euler sine/Fourier pseudospectral method and a time-splitting sine/Fourier pseudospectral method were proposed and applied with different approaches approximating the Hartree potential. Those approaches considered in this paper include: (1) fast convolution algorithms to evaluate the convolution of Laplacian kernel with density, which are accelerated with the help of FFT in 1D and fast multipole method (FMM) in higher dimensions; (2) a sine pseudospectral method to discretize a Poisson equation with homogeneous Dirichlet boundary conditions; (3) a Fourier pseudospectral method to discretize a Poisson equation with periodic boundary conditions. For the last approach, due to the inconsistency in 0-mode after taking Fourier transformation, the error from the truncated computation domain dominates the whole process and the approximation will converge as

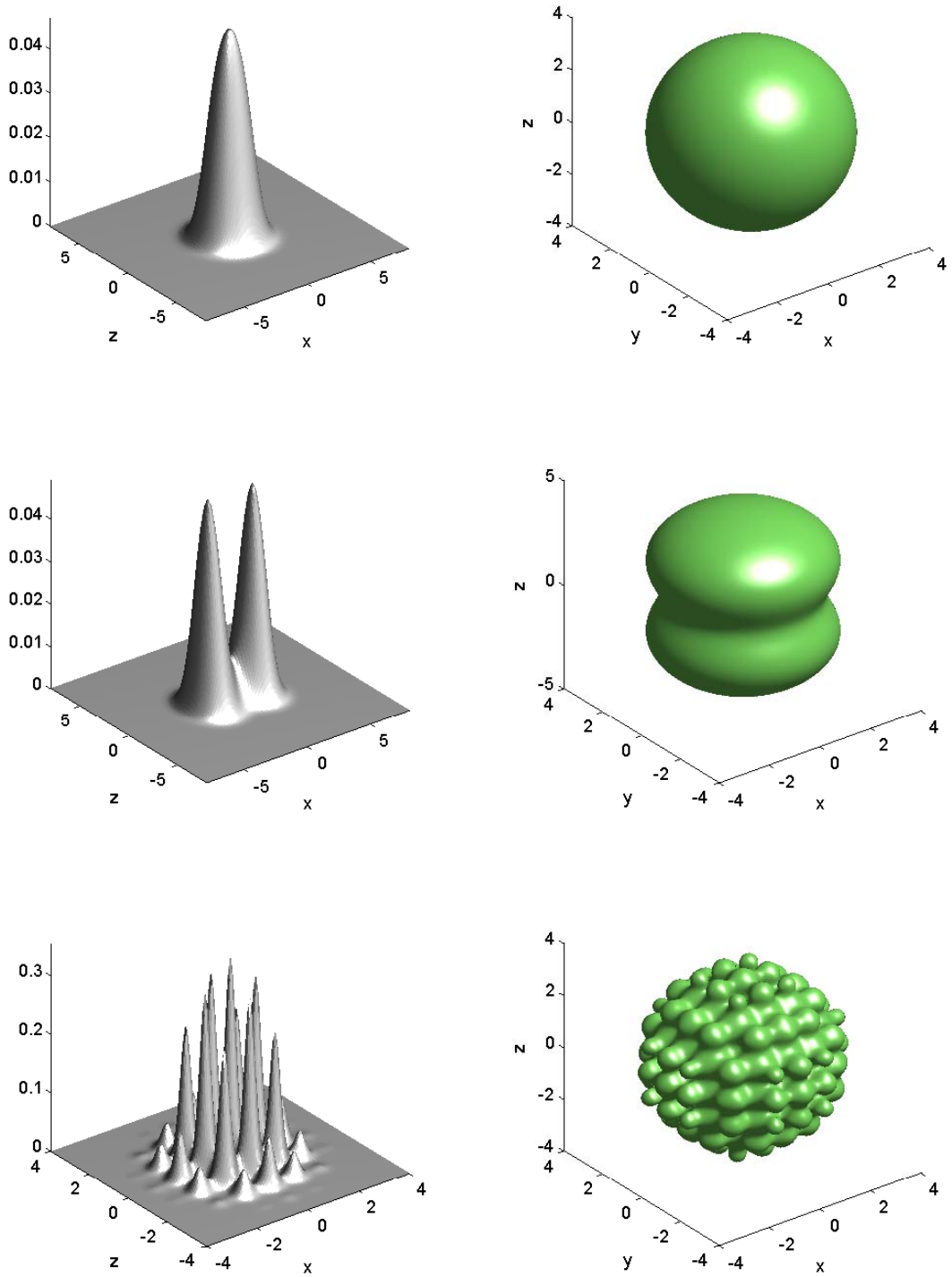

Figure 4: Surface plots of ground state $|\phi_g(x,0,z)|^2$ (left column) and isosurface plots of $|\phi_g(x,y,z)| = 0.01$ (right column) of SPS system (1.1) with $C_P = 100$ and $\alpha = 1$ under harmonic potential (top row), double-well potential (middle row) and optical lattice potential (bottom row).

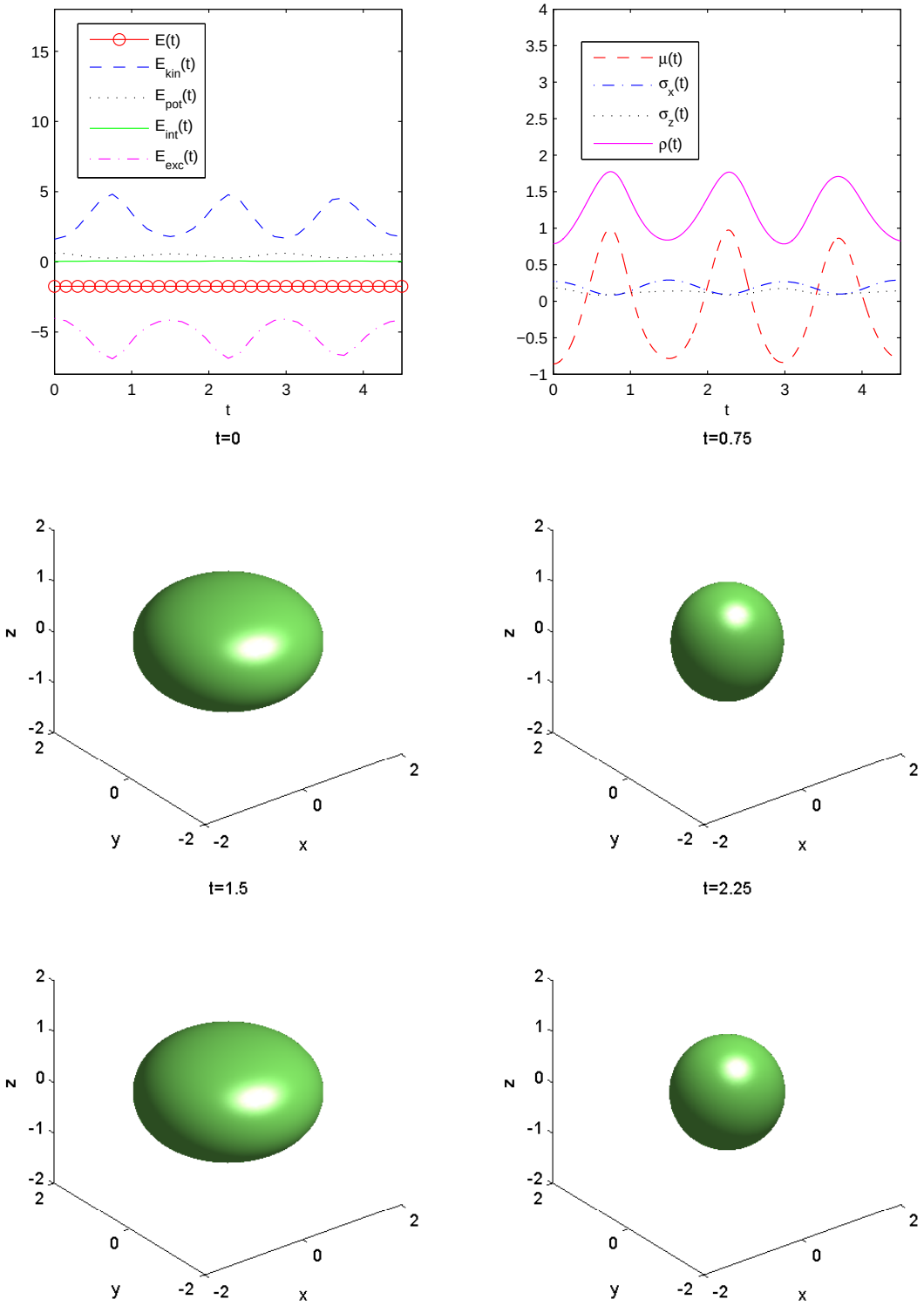

Figure 5: Time evolution of various quantities and isosurface plots of density $\rho(\mathbf{x}, t) := |\psi(\mathbf{x}, t)|^2 = 0.01$ at different time points for 3D SPS with slater coefficient changing from $\alpha = 5$ to $\alpha = 10$ at $t = 0$.

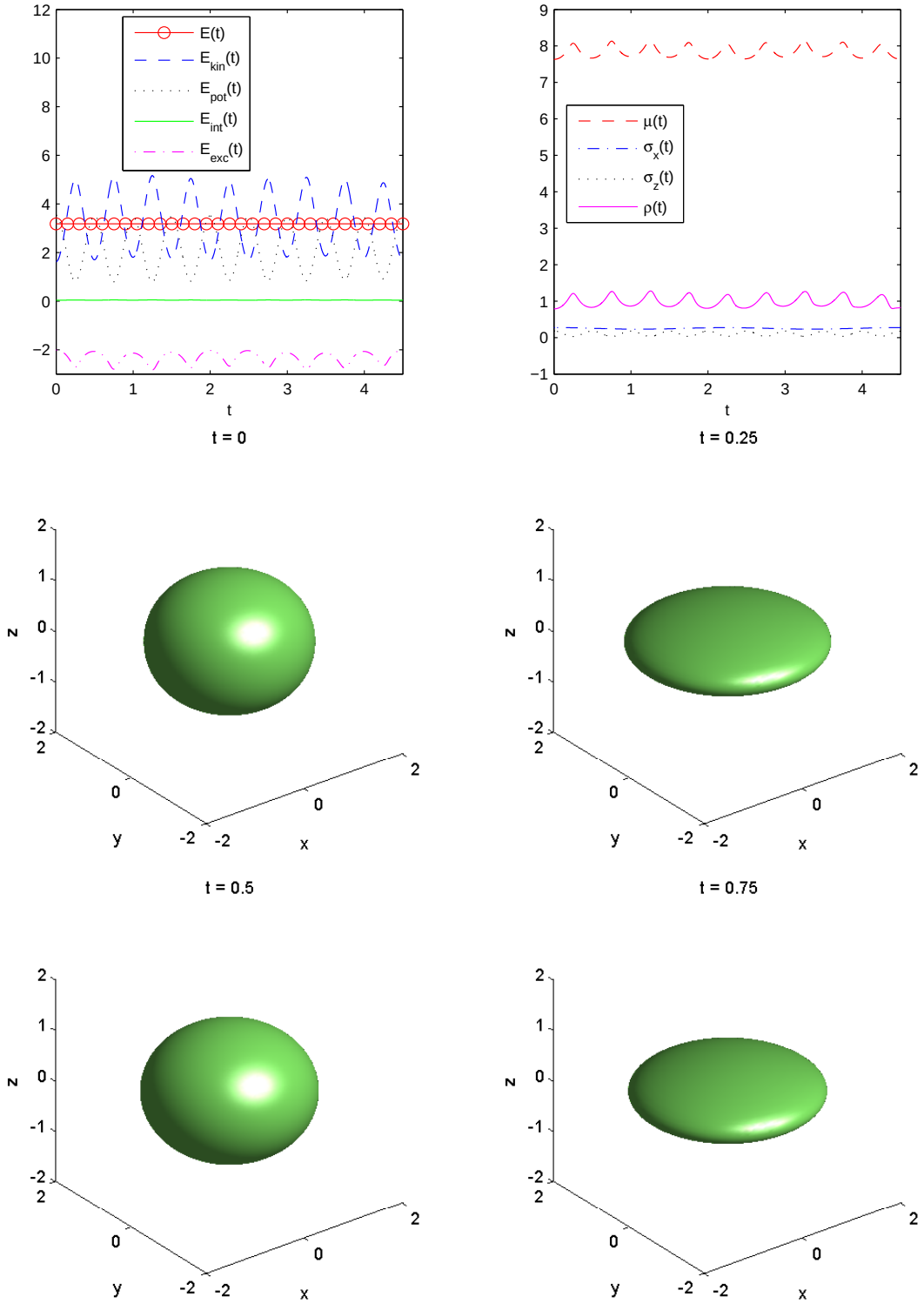

Figure 6: Time evolution of various quantities and isosurface plots of density $\rho(\mathbf{x}, t) := |\psi(\mathbf{x}, t)|^2 = 0.01$ at different time points for 3D SPS under external potential changing from $V_{\text{ext}} = \frac{1}{2}(x^2 + y^2 + 4z^2)$ to $V_{\text{ext}} = \frac{1}{2}(x^2 + y^2 + 36z^2)$ at $t = 0$.

the domain is chosen larger. This can be seen from the formulation of method as well as numerical experiment results. Detailed numerical comparisons also showed that in 1D the fast convolution and sine pseudospectral approaches are compatible, both achieving spectral order of accuracy in space, while in 3D the fast convolution based on FMM is second-order accurate and the Fourier pseudospectral approach is better than it in both efficiency and accuracy aspects. In conclusion, the sine pseudospectral approach is the best choice among all the ones discussed here. Lastly, we apply the backward Euler and time-splitting time integration with the sine pseudospectral spatial discretization to compute the ground states and dynamics of 3D SPS system in various setups.

The results in this paper pave a way for further numerical studies of the coupled Schrödinger-Poisson type systems arising in quantum physics area. However, it is noted that the methods proposed here cannot be extended to the governing systems with discontinuous coefficients, for example, the relevant systems arising in semiconductor area. This is because the derivation and high-order accuracy of the spectral-type space discretization highly depend on the high regularity of functions. In this case, other methods, like finite difference, finite element or spectral element approaches, would be the potential alternatives, and the detailed investigation is of course an interesting topic for further studies.

Acknowledgments

This work was supported in part by Academic Research Fund of Ministry of Education of Singapore grant R-146-000-120-112 (Y.Z. and X.D.), Chinese Scholarship Council (Y.Z.) and DEASE: MEST-CT-2005-021122 (Y.Z.). The authors would like to acknowledge the stimulating and helpful discussions with Prof. Weizhu Bao on the topic. This work was partially done while the authors were visiting the Institute for Mathematical Sciences, National University of Singapore, in 2009. The author (Y.Z.) is also grateful to Prof Norbert J. Mauser for his helpful suggestions and warm hospitality and support when he visited Wolfgang Pauli Institute, 2010. Also, the authors thank the anonymous referees for their constructive comments and helpful suggestions on the early manuscript. The computation results presented have been achieved in part by using the Vienna Scientific Cluster.

References

[1] N. Angelescu, M. Pulvirenti, A. Teta, Derivation and classical limit of a mean field equation for a quantum Coulomb system: Maxwell-Boltzmann statistics, J. Stat. Physics 74 (1994) 147-165.

[2] C. Bardos, L. Erdös, F. Golse, N.J. Mauser, H.T. Yau, Derivation of the Schrödinger-Poisson equation from the quantum N-particle Coulomb problem, C. R. Acad. Sci. Paris, Ser. I 334 (2002) 515-520.

[3] C. Bardos, F. Golse, N.J. Mauser, Mean field dynamics of fermions and the time-dependent Hartree-Fock equation, J. d. Mathématiques Pures et Appl. 82 (2003) 665-683.

[4] C. Bardos, A. Gottilieb, F. Golse, N.J. Mauser, Derivation of the time-dependent Hartree-Fock equation: the Coulomb interaction case, manuscript.

[5] W. Bao, Y. Cai, H. Wang, Efficient numerical methods for computing ground states and dynamics of dipolar Bose-Einstein condensates, J. Comput. Phys. 229 (2010) 7874-7892.

[6] W. Bao, I-L. Chern, F.Y. Lim, Efficient and spectrally accurate numerical methods for computing ground and first excited states in Bose-Einstein condensates, J. Comput. Phys. 219 (2006) 836-854.

[7] W. Bao, Q. Du, Computing the ground state solution of Bose-Einstein condensates by a normalized gradient flow, SIAM J. Sci. Comput. 25 (2004) 1674-1697.

[8] W. Bao, N.J. Mauser, H.P. Stimming, Effective one particle quantum dynamics of electrons: A numerical study of the Schrödinger-Poisson-Xα model, Comm. Math. Sci. 1 (2003) 809-831.

[9] W. Bao, S. Jin, P.A. Markowich, Time-splitting spectral approximations for the Schrödinger equation in the semiclassical regime, J. Comput. Phys. 175 (2002) 487-524.

[10] W. Bao, S. Jin, P.A. Markowich, Numerical studies of time-splitting spectral discretizations of nonlinear Schrödinger equations in the semiclassical regime, SIAM J. Sci. Comput. 25 (2003) 27-64.

[11] W. Bao, Y. Zhang, Dynamics of the ground state and central vortex states in Bose-Einstein condensation, Math. Models Meth. Appl. Sci. 15 (2005), 1863-1896.

[12] N. Ben Abballan, P. Degond, P.A. Markowich, On a one-dimensional Schrödinger-Poisson scattering model, ZAMP 48 (1997) 35-55.

[13] O. Bokanowski, B. Grébert, N.J. Mauser, Local density approximation for the energy of a periodic Coulomb model, Math. Meth., and Mod. in the Appl. Sci. 13 (8) (2003) 1185-1217.

[14] O. Bokanowski, N.J. Mauser, Local approximation for the Hartree-Fock exchange potential: a deformation approach, Math. Meth. and Mod. in the Appl. Sci. 9 (6) (1999) 941-961.

[15] O. Bokanowski, J.L. López, J. Soler, On a exchange interaction model for quantum transport: The Schrödinger-Poisson-Slater system, Math. Model Methods Appl. Sci. 12 (10) (2003) 1397-1412.

[16] J. Bourgain, Global solutions of nonlinear Schrödinger equations, AMS, 1999.

[17] T. Cazenave, Semilinear Schröinger equations, Courant Lecture Notes in Mathematics, vol. 10, New York University Courant Institute of Mathematical Sciences AMS, 2003.

[18] C. Cheng, Q. Liu, J. Lee, H.Z. Massoud, Spectral element method for the Schrödinger-Poisson system, J. Comput. Electron. 3 (2004) 417-421.

[19] H. Cheng, L. Greengard, V. Rokhlin, A fast adaptive multipole algorithm in three dimensions, J. Comput. Phys. 155 (1999) 468-498.

[20] P. Choquard, J. Stubbe, M. Vuffray, Stationary solutions of the Schrödinger-Newton Model-An ODE approach, Diff. Int. Eqns. 21 (2008) 665-679.

[21] P.A.M. Dirac, Note on exchange phenomena in the Thomas-Fermi atom, Proc. Cambridge Pilos. Soc. 26 (1931) 376-385.

[22] R. M. Dreizler, E.K.U. Gross, Density functional theory, Springer, Berlin, 1990.

[23] M. Ehrhardt, A. Zisowsky, Fast calculation of energy and mass preserving solutions of Schrödinger-Poisson systems on unbounded domains, J. Comput. Appl. Math. 187 (2006) 1-28.

[24] F. Ethridge, L. Greengard, A new fast-multipole accelerated Poisson solver in two dimensions, SIAM J. Sci. Comput. 23 (3) (2001) 741-760.

[25] L. Greengard, V. Rokhlin, A fast algorithm for particle simulations, J. Comput. Phys. 73 (1987) 325–348.

[26] L. Greengard, V. Rokhlin, A new version of the fast multipole method for the Laplace equation in three dimensions, Acta Numerica 6 (1997) 229-269.

[27] R. Harrison, I.M. Moroz, K.P. Tod, A numerical study of Schrödinger-Newton equations, Nonlinearity 16 (2003) 101-122.

[28] T. Hrycak, V. Rokhlin, An improved fast multipole algorithm for potential fields, SIAM J. Sci. Comput. 19 (1998) 1804-1826.

[29] E. H. Lieb, Thomas-Fermi and related theories of atoms and molecules, Rev. Modern Phys. 55 (1981) 603-641.

[30] E. H. Lieb, Existence and uniqueness of the minimizing of Choquards' nonlinear equation, Studies in Appl. Math. 57 (1976/77) 93-105.

[31] E. H. Lieb, B. Simon, The Thomas-Fermi theory of atoms, molecules, and solids, Adv. Math. 23 (1977) 22-116.

[32] P. L. Lions, Solution of Hartree-Fock equations for Coulomb systems, Comm. Math. Phys. 109 (1987) 33-97.

[33] S. Masaki, Energy solution to Schrödinger-Poisson system in the two-dimensional whole space, manuscript.

[34] N.J. Mauser, The Schrödinger-Poisson-X^α equation, Appl. Math. Lett. 14 (2001) 759-763.

[35] Ó. Sánchez, J. Soler, Long-Time Dynamics of the Schrödinger-Poisson-Slater Systems, J. Statist. Phys. 114 (2004) 179-204.

[36] J. Shen, T. Tang, Spectral and High-Order Methods with Applications, Science Press, Beijing, 2006.

[37] J.C. Slater, A simplification of the Hartree-Fock method, Phys. Rev. 81 (1951) 385-390.

[38] H.P. Stimming, The IVP for the Schrödinger-Poisson-Xα equation in one dimension, Math. Models Methods Appl. Sci. 15 (2005) 1169-1180.

[39] G. Strang, On the construction and comparison of difference schemes, SIAM J. Numer. Anal. 5 (1968) 505-517.

[40] C. Sulem, P.-L. Sulem, The nonlinear Schrödinger equation: self-focusing and wave collapse, Springer, 1999.

[41] K.I. Yoshida, Applications of Fast Multipole Method to Boundary Integral Equation Method, Ph.D thesis, 2001.

[42] D.G. Zhao, J.F. Huang, Y. Xiang, A new version Fast Multipole Method for evaluating the stress field of dislocation ensembles, Modeling Simul. Mater. Sci. Eng. 18(4) (2010).